

# Prediction of a Heusler alloy with switchable metal-to-half-metal behavior

Vasiliy D. Buchelnikov<sup>1,2</sup>, Vladimir V. Sokolovskiy<sup>1,2</sup>, Olga N. Miroshkina<sup>1,3,4</sup>,  
Danil R. Baigutlin<sup>1,3</sup>, Mikhail A. Zagrebin<sup>1,2,5</sup>, Bernardo Barbiellini<sup>3,6</sup>, and Erkki Lähderanta<sup>3</sup>

<sup>1</sup>*Faculty of Physics, Chelyabinsk State University, 454001 Chelyabinsk, Russia*

<sup>2</sup>*National University of Science and Technology "MISiS", 119049 Moscow, Russia*

<sup>3</sup>*Department of Physics, School of Engineering Science,  
LUT University, FI-53850 Lappeenranta, Finland*

<sup>4</sup>*Faculty of Physics and Center for Nanointegration Duisburg-Essen (CENIDE),  
University of Duisburg-Essen, 47048 Duisburg, Germany*

<sup>5</sup>*National Research South Ural State University, 454080 Chelyabinsk, Russia and*

<sup>6</sup>*Physics Department, Northeastern University, Boston, Massachusetts 02115, USA*

(Dated: February 16, 2021)

We propose a ferromagnetic Heusler alloy that can switch between a metal and a half-metal. This effect can provide tunable spintronics properties. Using the density functional theory (DFT) with reliable implementations of the electron correlation effects, we find  $\text{Mn}_2\text{ScSi}$  total energy curves consisting of distinct branches with a very small energy difference. The phase at low lattice crystal volume is a low magnetic half-metallic state while the phase at high lattice crystal volume is a high magnetic metallic state. We suggest that the transition between half-metallic and metallic states can be triggered by a triaxial contraction/expansion of the crystal lattice or by an external magnetic field if we assume that the lattice is cubic and remains cubic under expansion/contraction. However, the phase at high volume can also undergo an austenite-martensite phase transition because of the presence of Jahn-Teller active  $3d$  electrons on the Mn atoms.

## I. INTRODUCTION

Nowadays, spintronics is a rapid-developing field of science and technology<sup>1-4</sup>, which aims to use the intrinsic spin of the electron and its associated magnetic moment in solid-state devices<sup>5,6</sup> including synchronized networks of spin-transfer oscillators<sup>7</sup>, spin-transfer torque<sup>8</sup> and magnetoelectric random access memory devices<sup>9,10</sup>, spin transfer nano-generators<sup>11</sup>, and spin holographic processors<sup>12</sup>. The efficiency of these devices is related directly to the level of spin injection from the electrodes to the semiconductors and to their degree of spin polarization<sup>13</sup>. Half-metallic (HM) ferromagnetic (FM) compounds are characterized by an energy gap in one spin direction at the Fermi level. They therefore exhibit metallic character in one spin-channel and semiconducting behavior in the other spin-channel<sup>14,15</sup>.

Among HM ferromagnets, the half- and full-Heusler alloys are of great interest because they usually demonstrate stable half-metallicity with high Curie temperature and spin polarization<sup>14,16,17</sup>. Nowadays, much attention is given to the wide variety of FM  $\text{Co}_2YZ$  ( $Y = \text{Fe}, \text{Mn}$  and  $Z = \text{Si}, \text{Ge}, \text{Sn}$ )<sup>18-26</sup>,  $\text{Fe}_2YZ$  ( $Y = \text{Cr}, \text{Mn}, \text{Co}$  and  $Z = \text{Si}, \text{Al}, \text{Ga}$ )<sup>13,27-29</sup> and ferrimagnetic (FIM)  $\text{Mn}_2YZ$  ( $Y = \text{V}, \text{Cr}, \text{Fe}, \text{Co}, \text{Ni}$  and  $Z = \text{Al}, \text{Ga}, \text{Si}, \text{Ge}, \text{Sn}, \text{In}$ )<sup>13,30-36</sup> that were studied both theoretically and experimentally. In the  $\text{Co}_2YZ$  family, the HM behavior appears when the  $Y$  element has less valence electrons than Co. On the other hand, the half-metallicity in  $\text{Fe}_2YZ$  and  $\text{Mn}_2YZ$  families occurs regardless the number of valence electrons in the  $Y$  atoms. Therefore, the HM behavior is promoted by the Mn and Fe atoms. Moreover, parallel or antiparallel spin alignment of two Mn atoms can lead to FM and FIM order and

to noncolinear configurations. Since the  $\text{Mn}^{3+}$  ion has a  $d^4$  electronic configuration with partially filled  $e_g$  orbitals, it is Jahn-Teller active. This effect explains the tetragonal distortion producing high magnetocrystalline anisotropy (MCA). This observation makes FIM  $\text{Mn}_2$ -based alloys useful for transfer torque application, where high MCA is a key factor for fast switching with low currents and high thermal stability<sup>37,38</sup>.

An interesting idea to add Sc (with one  $d$  valence electron) into the matrix of the  $\text{Mn}_2$ -based family has been recently proposed by Ram *et al.*<sup>13</sup>. These authors performed DFT calculations for  $\text{Mn}_2\text{Sc}Z$  ( $Z = \text{Si}, \text{Ge}, \text{Sn}$ ) Heusler alloys taking in account on-site Coulomb interaction effects. The results indicated HM behavior with a narrow band gap in the case of  $\text{Mn}_2\text{ScSi}$  and  $\text{Mn}_2\text{ScGe}$  whereas  $\text{Mn}_2\text{ScSn}$  displayed metallic behavior. Ram *et al.*<sup>13</sup> claimed that one must use an accurate DFT scheme to reproduce their results since the deficiencies of traditional DFT exchange correlation approximations such as the local spin density approximation (LSDA) and the generalized gradient approximation (GGA) prevent the appearance of HM properties in  $\text{Mn}_2\text{Sc}Z$  alloys. Therefore, one must reduce the self interaction errors present in LSDA and GGA by using schemes such as the DFT+ $U$  method<sup>39</sup>. Recently, we have studied correlation effects beyond the GGA in  $\alpha\text{-Mn}$ <sup>40</sup>,  $\text{Ni}_2$ - and  $\text{Co}_2$ -based Heusler alloys<sup>25,41</sup> by using the strongly constrained and appropriately normed (SCAN) functional<sup>42</sup> (meta-GGA method), which contains self-interaction correction without introducing an explicit Hubbard parameter  $U$ .

In this work, we confirm that reliable corrections beyond the GGA not only stabilize the HM properties of the  $\text{Mn}_2\text{ScSi}$  alloys in a robust way but reveal a surpris-

ingly rich phase diagram useful for tunable spintronics applications. For example, one could produce spintronic logic devices with switches that can operate on femtosecond time scales<sup>43</sup>. Our results show that  $\text{Mn}_2\text{ScSi}$  is an exemplar magnetic functional material hosting competing phases. The lattice of this material provides an elastic environment where charge, spin, and orbital degrees of freedom interact and produce unexpected functionalities<sup>44</sup>. Small energy differences between phases also offer unique opportunities to benchmark Coulomb correlation effects in DFT.

The outline of the paper is as follows. Section II contains the calculation details. Section III is devoted to the discussion of the results of structural, magnetic, and electronic properties and phase stability of  $\text{Mn}_2\text{ScSi}$ . The concluding remarks are presented in Sec. IV.

## II. CALCULATION DETAILS

To perform the calculations, we employed the PAW method implemented in VASP code<sup>45,46</sup> using 16-atom supercells. The GGA for the exchange correlation functional was treated within the Perdew, Burke, and Ernzerhof (PBE)<sup>47</sup> scheme. Electron correlation effects beyond GGA were included using both GGA+ $U$  by Dudarev *et al.*<sup>48</sup> and meta-GGA SCAN by Sun *et al.*<sup>42</sup>. The parameter  $U$  for Mn is taken in the interval from 0.2 to 2 eV. The value  $U_{\text{Mn}} = 1.973$  eV was chosen in accordance with Ram *et al.*<sup>13</sup>. Since the Coulomb correlation for Sc affects weakly the electronic and magnetic properties, we choose  $U_{\text{Sc}} = 0.435$  eV proposed by Ram *et al.*<sup>13</sup>. The volume optimization of regular and inverse Heusler structures (space groups  $Fm\bar{3}m$  and  $F\bar{4}3m$ ) with different magnetic order is perform. For all functionals, the geometry optimization procedure yields the regular  $L2_1$ -cubic Heusler structure as the most favorable one with the FIM order involving antiparallel alignment of Mn and Sc magnetic moments (see Supplementary Material (SM)<sup>49</sup>).

## III. RESULTS AND DISCUSSIONS

### A. Structural optimization

We first consider the total energy results. In Fig. 1, we show the total energy as a function of the lattice constant ( $a$ ) and the total magnetic moment ( $\mu_{\text{tot}}$ ) calculated within SCAN and GGA+ $U$ . SCAN yields a degenerated ground state with two almost equal energy minima observed at lattice constants of 5.905 and 6.108 Å. These two minima correspond to two magnetic states with the values of  $\mu_{\text{tot}}$  equal to 3 and 5.8  $\mu_B/\text{f.u.}$  as shown in Fig. 1(b). We denote these states as the low-magnetic state (LMS) and high-magnetic state (HMS), respectively. The energy and magnetic moment differences between LMS and HMS are  $\Delta E = 3.75$  meV/atom

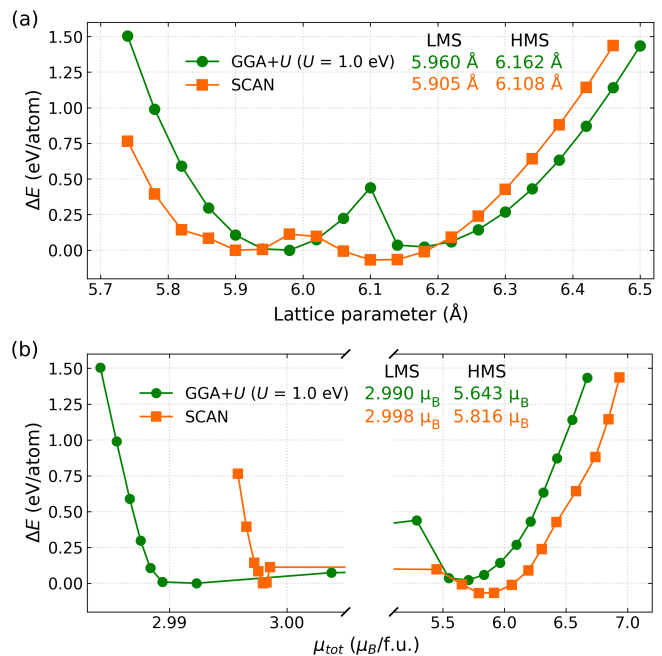


FIG. 1. The total energy difference ( $\Delta E$ ) as a function of (a) lattice parameter and (b) magnetic moment of  $\text{Mn}_2\text{ScSi}$  for SCAN and GGA+ $U$  ( $U = 1$  eV) solutions. For each cases, the  $\Delta E$  is plotted with respect to the left energy minimum.

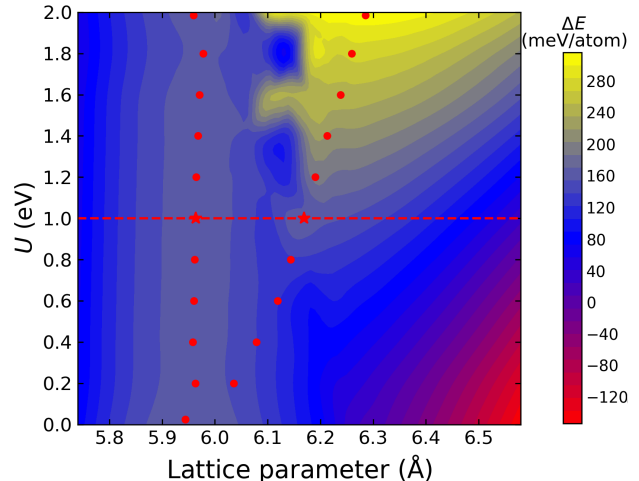


FIG. 2. The total energy difference for  $\text{Mn}_2\text{ScSi}$  calculated by GGA+ $U$  for a set of  $U$  values and mapped into the diagram «Coulomb repulsion term ( $U$ ) – lattice parameter ( $a$ )».  $\Delta E$  is plotted with respect to the minimum for LMS. The optimized lattice parameters, which are estimated from the fitting for the Birch-Murnaghan equation of state for both LMS and HMS, are marked by the red symbols. The stars denote degeneracy of the ground state for which the LMS and HMS have a similar energy at  $U = 1$  eV.

and  $\Delta\mu = 2.90 \mu_B/\text{f.u.}$ , respectively. The total magnetic moment in SCAN is an integer in agreement with the empirical Slater-Pauling (SP)<sup>50</sup> rule thereby revealing the HM behavior.

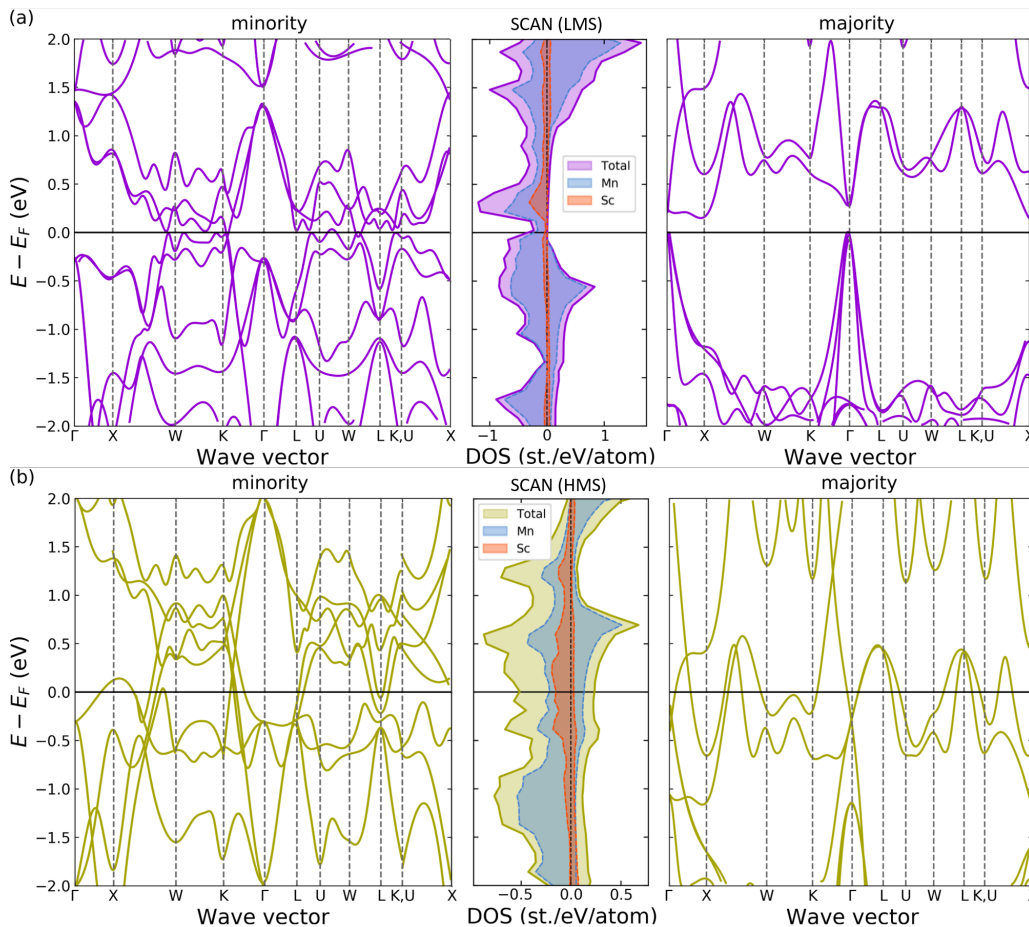


FIG. 3. SCAN energy band structure, total and partial DOSs of  $\text{Mn}_2\text{ScSi}$  calculated for the (a) LMS and (b) HMS with the optimized lattice constants  $a_0^{\text{LMS}} = 5.905 \text{ \AA}$  and  $a_0^{\text{HMS}} = 6.108 \text{ \AA}$ , respectively.

In contrast to SCAN, our GGA calculations give only one clear minima at lattice constant  $a_0 = 5.94 \text{ \AA}$ . Ram *et al.*<sup>13</sup> have only considered GGA+ $U$  corrections around the GGA total energy minima but they have missed the second total energy minima at higher volume. In our case, the volume optimization with fixed  $U$  value of 1.973 eV as Ram *et al.*<sup>13</sup> yields both a local energy minimum at a similar equilibrium volume as GGA and the global minimum at larger volume as illustrated in the SM<sup>49</sup>.

To understand better these results, we performed a parametric study of the Hubbard parameter  $U$ . Figure 2 illustrates a contour map of the total energy as functions of  $U$  and lattice parameter  $a$ . The set of  $E(a)$  curves for various  $U$  is given in the SM<sup>49</sup>. We delineate in this contour map shown in Fig. 2 a triangle linking optimized lattice constants at local and global energy minima corresponding to the LMS and HMS, respectively. The vertex of this triangle is located close to  $U$  equal zero demonstrating that GGA is a singular point in terms of correlation effects. As soon as we introduce a small  $U$  value, two well defined structures with different magnetization appear in the energy landscape. Related parametric studies

in  $\gamma$ -Mn by Podloucky and Redinger<sup>51</sup> and by Pulkkinen *et al.*<sup>40</sup> have found that  $U$  approximately 1 eV gives the corrected equilibrium volume. Therefore, we believe that  $U \approx 1 \text{ eV}$  is a correct energy scale to describe the correlation effects in the present case. For  $U = 1 \text{ eV}$ , the LMS and HMS are found to be close to each other in the energy as shown in Fig 1(a) in agreement with SCAN.

The transition between LMS and HMS can be achieved by a uniform contraction/expansion of the crystal lattice by  $\approx 3.3 \%$ . We predict that the magnetovolume effect<sup>52</sup> ( $\frac{\Delta V}{V_{\text{HMS}}}$ ) should be accompanied by in the change in magnetization ( $\Delta\mu_{\text{tot}}$ ) corresponding to  $\approx 2.8 \mu_B/\text{f.u.}$  as it is derived from SCAN calculations. For GGA+ $U$  with  $U = 1 \text{ eV}$ ,  $\Delta\mu_{\text{tot}}$  is slightly less and equals to  $\approx 2.7 \mu_B/\text{f.u.}$  Another way is to switch the transition by applying magnetic field.

## B. Electronic structure

To understand the electronic structure, we consider the spin-polarized band structures and the density of states (DOS). The bands are calculated along the high-

symmetric points of the first Brillouin zone for the majority and minority spin channels for the GGA, GGA+ $U$ , and SCAN methods. In Fig. 3, we present both the SCAN bands and DOS curves calculated at the optimized lattice constants for LMS and HMS found in Fig. 1(a). The corresponding figures for GGA and GGA+ $U$  are given in the SM<sup>49</sup>. As Fig. 3(a) suggests, in the case of LMS, the minority-spin bands present few band crossings at the Fermi level ( $E_F$ ), while the majority-spin bands reveal an clear energy gap around  $E_F$ . Such HM behavior for  $\text{Mn}_2\text{ScSi}$  is quite different of that in regular HM Heusler alloys in which the spin up states are filled and the spin down states are unoccupied at  $E_F$ <sup>37</sup>. The energy gap at  $\Gamma$  point for the majority bands is direct as shown in Fig. 3(a) and its predicted value within SCAN is 0.32 eV which is twice the value calculated by Ram *et al.*<sup>13</sup>.

In terms of the HMS (Fig. 3(b)), both the minority and majority spin bands as well as DOSs show clear metallic behavior. It is important to notice that the bands calculated for the GGA+ $U$  with  $U = 1.973$  eV at the optimized volume<sup>49</sup> display metallic character in contrast to the bands reported by Ram *et al.*<sup>13</sup> indicating that the HM properties is lost for the larger volume. Therefore, it is possible to switch the HM behavior by a uniform contraction/expansion of the crystal lattice.

Such switching behavior can be rationalized by analyzing the 3d partial DOSs for Mn atoms in the vicinity of  $E_F$  shown in Fig. 4. For the LMS, three  $t_{2g}$  orbitals at  $E_F$  are present in the minority spin channel and contributed to the integer magnetic moment, whereas two  $e_g$  orbitals are almost empty. In contrast, both the  $t_{2g}$  and  $e_g$  orbitals at  $E_F$  for the minority spin channel are occupied for the HMS. For the majority spin channel we observe mostly  $e_g$  orbitals. The main difference between LMS and HMS is the occupation of an energy  $e_g$  peak for the majority spin band. When the  $e_g$  state is occupied the system undergoes an austenitic-martensite transition because of Jahn-Teller effects.

Our results above apply if the lattice is cubic and remains cubic under triaxial expansion/contraction<sup>53</sup>. To examine the martensitic phase, we have performed total energy calculations as a function of tetragonal distortion ratio  $c/a$  assuming a constant volume between austenite ( $c/a = 1$ ) and martensite ( $c/a \neq 1$ ). Indeed the martensitic phase with  $c/a = 1.27$  is found to be energetically favorable<sup>49</sup>. The predicted  $\Delta\mu_{tot}$  between austenitic and martensitic phase is about  $1.807 \mu_B/\text{f.u.}$  This finding allows us to conclude that  $\text{Mn}_2\text{ScSi}$  should also display magnetocaloric properties in the vicinity of magnetostructural phase transformation<sup>54</sup>.

### C. Phase stability

Since the predicted  $\text{Mn}_2\text{ScSi}$  compound has not yet been grown, it is important to evaluate its phase stability. We have therefore checked the thermodynamic stability in three steps.

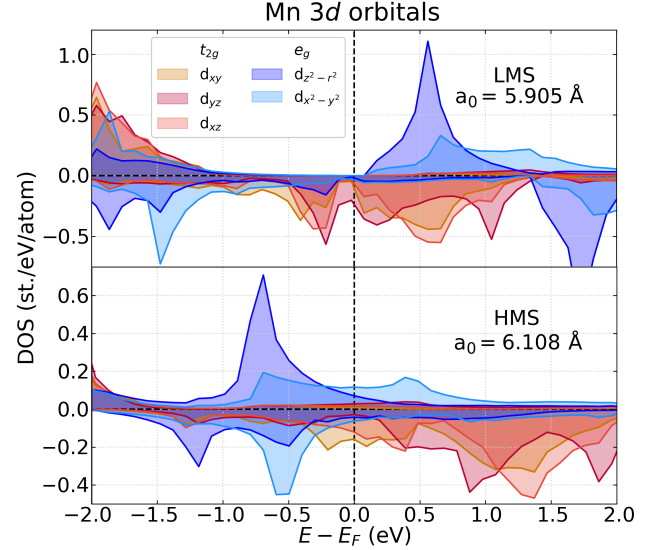


FIG. 4. Mn-3d orbital resolved DOSs for LMS (upper) and HMS (bottom) calculated with SCAN.

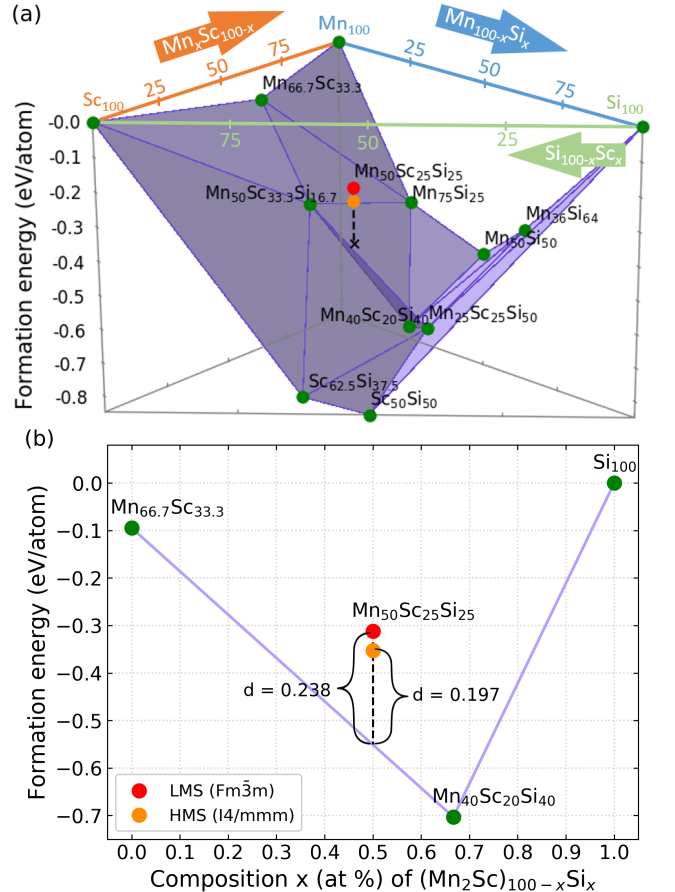


FIG. 5. (a) The hull energy convex and (b) cross section of hull energy convex that contains the convex hull distance for  $\text{Mn}_2\text{ScSi}$  with the LMS cubic structure and HMS tetragonal one. The formation energies are calculated with SCAN.

As a preliminary test, we have performed formation energy ( $E_{form}$ ) calculations for  $Mn_2ScSi$  with respect to the elemental components in their groundstate bulk structures. The negative values of  $E_{form}^{SCAN}$  ( $-0.312$  and  $-0.319$  eV/atom for LMS and HMS, respectively) indicate thermodynamic stability of  $Mn_2ScSi$  in the corresponding cubic states<sup>49</sup>.

However, stability with respect to the sum of total energies of the corresponding pure elements is a necessary but not yet a sufficient condition for thermodynamic phase stability. In order to clarify this point, we must compare also  $E_{form}$  of a compound against to all stable combination of phases at that composition. This aim can be achieved with the convex hull construction for the phase space of interest<sup>55</sup>. Typically, a convex hull connects stable phases that are lower in  $E_{form}$  than any other phase under consideration in this overall composition. In this way, phases located above the convex hull are metastable or unstable while phases placed on the convex hull are stable. The pivot points (12 stable phases) for the convex hull of the Mn-Sc-Si ternary system were taken according to the AFLOW database<sup>55</sup> (they are listed in Table 2 of SM<sup>49</sup>). By considering the  $E_{form}^{SCAN}$  of these phases, we constructed the three-dimensional convex hull shown in Fig. 5(a). Here, we indicate  $E_{form}^{SCAN}$  for  $Mn_2ScSi$  with the LMS cubic structure and HMS tetragonal one. The formation energies of pure elements are set to zero. We show the cross section of the hull energy convex in Fig. 5(b) to estimate the distance from the most stable phase. The  $Mn_2ScSi$  is located above the convex hull by  $\approx 0.24$  eV/atom for LMS cubic phase as shown in Fig. 5(b). Interestingly, this distance is about 0.188 eV/atom<sup>55</sup> (<http://www.afLOWlib.org>) for GGA-PBE. Thereby, this result suggests a metastable tendency of the  $Mn_2ScSi$  compound.

In order to understand this metastable behavior, we compare the  $Mn_2ScSi$  phase energy to the energies of decomposition products (pivot points of the convex hull) at that composition and calculate the mixing energy  $E_{mix}$ . To accomplish this task, we consider 23 possible decomposition reactions into the three stable components (see Table 3 and Fig. 7 in SM<sup>49</sup>). As a result, we found that 9 of 23 reactions yield a negative sign  $E_{mix}$  indicating the stability of LMS cubic phase against to segregation process. Therefore, we conclude that  $Mn_2ScSi$  can be grown as a metastable compound. We must keep in mind that the well-known  $Ni_2Mn_{1+x}Z_{1-x}$  Heusler alloys show both experimentally and theoretically a segregation tendency into ternary stoichiometric and binary compounds<sup>56-59</sup> due to several-step heat treatment. Despite this metastable character,  $Ni_2Mn$ -based alloys still exhibit remarkable multi-functional properties.

## IV. CONCLUSION

In conclusion, accurate DFT calculations in  $Mn_2ScSi$  Heusler alloy reveals an almost equal double energy minima behavior for close lattice constants but different magnetic moments.  $Mn_2ScSi$  displays either half-metallic (in LMS) or metallic (in HMS) behavior as a function of the lattice parameter. Our study shows how one can preserve the HM phase or one can switch to the metallic phase. We suggest that the half-metallic  $\leftrightarrow$  metallic transition might be realized by applying an external magnetic field or pressure. The critical magnetic field evaluated from the relation between  $\Delta E$  and Zeeman energy is about 11 T. While the magnetovolume effect and critical pressure are predicted to be 3.3% and 20 GPa, respectively. A second interesting aspect of the correlation effects is related to the prediction of an austenite-martensite transformation for the metallic phase, which produces a change in magnetization and a magnetocaloric effect.

We suggest that the switching mechanism between half-metallic and metallic behavior could be implemented for the design of spintronics devices like spin filters, sensors, switches, logical gates with femtosecond time scale<sup>43</sup>. Till date many studies have been performed theoretically and experimentally to investigate the externally controlled carrier's spin polarization and half-metallic-metallic transition in HM Heusler alloys by applying pressure, magnetic or electric fields<sup>25,60-62</sup>. However, in all these cases, the external load was applied for a certain length of time, which implies significant energy consumption. In the present work, the proposed switching behavior in  $Mn_2ScSi$  can be realized at once. Since this external perturbation is limited in time, the energy consumption is significantly lowered. This finding opens new avenues for fast and energy efficient spintronics applications.

## V. ACKNOWLEDGMENTS

SCAN calculations were supported by the RSF - Russian Science Foundation project No. 17-72-20022. GGA calculations were performed with the support of the Ministry of Science and Higher Education of the Russian Federation within the framework of the Russian State Assignment under contract No. 075-00250-20-03. GGA+ $U$  calculations were funded by the RFBR - Russian Foundation for Basic Research No. 20-42-740006. B.B. acknowledges CSC-IT Center for Science, Finland, for computational resources and support from the COST Action CA16218. O.N.M. acknowledges the Deutsche Forschungsgemeinschaft (DFG, German Research Foundation) - Project-ID 405553726 - TRR 270, subproject B06. V.D.B. and M.A.Z. gratefully acknowledge the financial support of the Ministry of Science and Higher Education of the Russian Federation in the framework of Increase Competitiveness Program of NUST "MISIS" (No. K2-2020-018), implemented by a governmental decree, N 211.

- <sup>1</sup> W. Gallagher, *Emerging Spintronic Memories* (CRC Press, 2019) pp. 443–470.
- <sup>2</sup> A. Fert, *Rev. Mod. Phys.* **80**, 1517 (2008).
- <sup>3</sup> B. Dieny, I. L. Prejbeanu, K. Garello, P. Gambardella, P. Freitas, R. Lehndorff, W. Raberg, U. Ebels, S. O. Demokritov, J. Akerman, *et al.*, *Nature Electronics* **3**, 446 (2020).
- <sup>4</sup> J. Puebla, J. Kim, K. Kondou, and Y. Otani, *Communications Materials* **1**, 1 (2020).
- <sup>5</sup> S. Bhatti, R. Sbiaa, A. Hirohata, H. Ohno, S. Fukami, and S. Piramanayagam, *Mater. Today* **20**, 530 (2017).
- <sup>6</sup> A. Hirohata, K. Yamada, Y. Nakatani, I.-L. Prejbeanu, B. Diény, P. Pirro, and B. Hillebrands, *J. Magn. Magn. Mater.* **509**, 166711 (2020).
- <sup>7</sup> J. Torrejon, M. Riou, F. A. Araujo, S. Tsunegi, G. Khalsa, D. Querlioz, P. Bortolotti, V. Cros, K. Yakushiji, A. Fukushima, *et al.*, *Nature* **547**, 428 (2017).
- <sup>8</sup> Y.-C. Liao, C. Pan, and A. Naemi, *IEEE Journal on Exploratory Solid-State Computational Devices and Circuits* **6**, 9 (2020).
- <sup>9</sup> H. Zhang, W. Kang, K. Cao, B. Wu, Y. Zhang, and W. Zhao, *IEEE Transactions on Electron Devices* **66**, 2017 (2019).
- <sup>10</sup> T. Wu, A. Bur, K. Wong, P. Zhao, C. S. Lynch, P. K. Amiri, K. L. Wang, and G. P. Carman, *Appl. Phys. Lett.* **98**, 262504 (2011).
- <sup>11</sup> L. Fu, Z. Cao, S. Hemour, K. Wu, D. Houssameddine, W. Lu, S. Pistorius, Y. Gui, and C.-M. Hu, *Appl. Phys. Lett.* **101**, 232406 (2012).
- <sup>12</sup> Y. K. Fetisov and A. S. Sigov, *RENSIT* **10**, 343 (2018).
- <sup>13</sup> M. Ram, A. Saxena, A. E. Aly, and A. Shankar, *RSC Adv.* **10**, 7661 (2020).
- <sup>14</sup> L. Bainsla and K. Suresh, *Appl. Phys. Rev.* **3**, 031101 (2016).
- <sup>15</sup> M. Shakil, H. Arshad, M. Zafar, M. Rizwan, S. S. A. Gillani, and S. Ahmed, *Molecular Physics* **118**, e1789770 (2020).
- <sup>16</sup> C. Palmstrøm, *MRS Bull.* **28**, 725 (2003).
- <sup>17</sup> H. Mori, Y. Odahara, D. Shigyo, T. Yoshitake, and E. Miyoshi, *Thin Solid Films* **520**, 4979 (2012).
- <sup>18</sup> D. Hoat, J. Rivas-Silva, and A. M. Blas, *Journal of Computational Electronics* **17**, 1470 (2018).
- <sup>19</sup> B. Deka, D. Chakraborty, and A. Srinivasan, *Physica B* **448**, 173 (2014).
- <sup>20</sup> L. Siakeng, G. M. Mikhailov, and D. Rai, *Journal of Materials Chemistry C* **6**, 10341 (2018).
- <sup>21</sup> R. Y. Umetsu, A. Okubo, and R. Kainuma, *J. Appl. Phys.* **111**, 073909 (2012).
- <sup>22</sup> D. Comtesse, B. Geisler, P. Entel, P. Kratzer, and L. Szunyogh, *Phys. Rev. B* **89**, 094410 (2014).
- <sup>23</sup> M. A. Zagrebin, V. V. Sokolovskiy, and V. D. Buchelnikov, *J. Phys. D Appl. Phys.* **49**, 355004 (2016).
- <sup>24</sup> M. Meinert, C. Friedrich, G. Reiss, and S. Blügel, *Phys. Rev. B* **86**, 245115 (2012).
- <sup>25</sup> O. N. Miroshkina, D. R. Baigutlin, V. V. Sokolovskiy, M. A. Zagrebin, A. Pulkkinen, B. Barbiellini, E. Lähderanta, and V. D. Buchelnikov, *J. Appl. Phys.* **127**, 175108 (2020).
- <sup>26</sup> I. Galanakis, K. Özdoğan, B. Aktaş, and E. Şaşıoğlu, *Appl. Phys. Lett.* **89**, 042502 (2006).
- <sup>27</sup> S. Chaudhuri, V. Srihari, A. Nigam, and P. Bhoje, *J. Appl. Phys.* **126**, 083904 (2019).
- <sup>28</sup> S. He, Y. Liu, Y. Zheng, Q. Qin, Z. Wen, Q. Wu, Y. Yang, Y. Wang, Y. Feng, K. L. Teo, *et al.*, *Phys. Rev. Mater.* **1**, 064401 (2017).
- <sup>29</sup> L. Hongzhi, Z. Zhiyong, M. Li, X. Shifeng, L. Heyan, Q. Jingping, L. Yangxian, and W. Guangheng, *J. Phys. D* **40**, 7121 (2007).
- <sup>30</sup> H. Luo, Z. Zhu, G. Liu, S. Xu, G. Wu, H. Liu, J. Qu, and Y. Li, *J. Magn. Magn. Mater.* **320**, 421 (2008).
- <sup>31</sup> H. Zenasni, H. Faraoun, and C. Esling, *J. Magn. Magn. Mater.* **333**, 162 (2013).
- <sup>32</sup> H. Luo, H. Zhang, Z. Zhu, L. Ma, S. Xu, G. Wu, X. Zhu, C. Jiang, and H. Xu, *J. Appl. Phys.* **103**, 083908 (2008).
- <sup>33</sup> V. V. Sokolovskiy, M. A. Zagrebin, Y. Sokolovskaya, and V. D. Buchelnikov, *Solid State Phenom.*, **233**, 229 (2015).
- <sup>34</sup> S. Chadov, X. Qi, J. Kübler, G. H. Fecher, C. Felser, and S. C. Zhang, *Nat. Mater.* **9**, 541 (2010).
- <sup>35</sup> T. Graf, S. S. P. Parkin, and C. Felser, *IEEE Trans. Magn.* **47**, 367 (2010).
- <sup>36</sup> A. K. Nayak, M. Nicklas, S. Chadov, P. Khuntia, C. Shekhar, A. Kalache, M. Baenitz, Y. Skourski, V. K. Guduru, A. Puri, *et al.*, *Nat. Mater.* **14**, 679 (2015).
- <sup>37</sup> C. Felser, L. Wollmann, S. Chadov, G. H. Fecher, and S. S. P. Parkin, *APL Mater.* **3**, 041518 (2015).
- <sup>38</sup> J. Winterlik, S. Chadov, A. Gupta, V. Alijani, T. Gasi, K. Filsinger, B. Balke, G. H. Fecher, C. A. Jenkins, F. Casper, *et al.*, *Adv. Mater.* **24**, 6283 (2012).
- <sup>39</sup> M. Cococcioni and S. De Gironcoli, *Phys. Rev. B* **71**, 035105 (2005).
- <sup>40</sup> A. Pulkkinen, B. Barbiellini, J. Nokelainen, V. Sokolovskiy, D. Baigutlin, O. Miroshkina, M. Zagrebin, V. Buchelnikov, C. Lane, R. S. Markiewicz, A. Bansil, J. Sun, K. Pussi, and E. Lähderanta, *Phys. Rev. B* **101**, 075115 (2020).
- <sup>41</sup> V. D. Buchelnikov, V. V. Sokolovskiy, O. N. Miroshkina, M. A. Zagrebin, J. Nokelainen, A. Pulkkinen, B. Barbiellini, and E. Lähderanta, *Phys. Rev. B* **99**, 014426 (2019).
- <sup>42</sup> J. Sun, A. Ruzsinszky, and J. P. Perdew, *Phys. Rev. Lett.* **115**, 036402 (2015).
- <sup>43</sup> P. Tengdin, C. Gentry, A. Blonsky, D. Zusin, M. Gentry, L. Hellbrück, M. Hofherr, J. Shaw, Y. Kvashnin, E. K. Delczeg-Czirjak, M. Arora, H. Nembach, T. J. Silva, S. Mathias, M. Aeschlimann, H. C. Kapteyn, D. Thonig, K. Koumpouras, O. Eriksson, and M. M. Murnane, *Sci. Adv.* **6** (2020).
- <sup>44</sup> T. Kakeshita, T. Fukuda, A. Saxena, and A. Planes, *Disorder and Strain-Induced Complexity in Functional Materials*, Vol. 148 (2011).
- <sup>45</sup> G. Kresse and J. Furthmüller, *Phys. Rev. B* **54**, 11169 (1996).
- <sup>46</sup> G. Kresse and D. Joubert, *Phys. Rev. B* **59**, 1758 (1999).
- <sup>47</sup> J. Perdew, K. Burke, and M. Ernzerhof, *Phys. Rev. Lett.* **77**, 3865 (1996).
- <sup>48</sup> S. Dudarev, G. Botton, S. Savrasov, C. Humphreys, and A. Sutton, *Phys. Rev. B* **57**, 1505 (1998).
- <sup>49</sup> See Supplemental Materials at <http://XXXXXX> for the additional information about calculation details and the results of *ab initio* ground state calculations for Mn<sub>2</sub>ScSi.
- <sup>50</sup> According to the SP rule for HM systems, the total magnetic moment is equal to  $\mu_{tot} = N_e - 24$ , where  $N_e$  is the total number of valence electrons. For Mn<sub>2</sub>ScSi,  $N_e$  is 21,

and so  $\mu_{tot} = 3\mu_B/\text{f.u.}$  by absolute value is expected. Notice, the negative sign of  $\mu_{tot}$  yields the energy gap at the Fermi level for majority density of states.

- <sup>51</sup> R. Podloucky and J. Redinger, *J. Phys. Condens. Matter* **31**, 054001 (2018).
- <sup>52</sup>  $\frac{\Delta V}{V_{HMS}} = \frac{V_{HMS} - V_{LMS}}{V_{HMS}}$ , here  $V_{HMS}$  and  $V_{LMS}$  are the volume cells of HMS and LMS, respectively.
- <sup>53</sup> We have checked the stability of LMS and HMS in a cubic phase to verify that the solution converges to the cubic lattice by considering a full structural relaxation using supercells with artificially broken symmetries. Our calculations have shown that the cubic symmetry is preserved for both LMS and HMS if the relaxation calculations are performed in the vicinity of corresponding optimized lattice constants  $a_0$ .
- <sup>54</sup> A. Planes, L. Mañosa, and M. Acet, *J. Phys. Condens. Matter* **21**, 233201 (2009).
- <sup>55</sup> C. Oses, E. Gossett, D. Hicks, F. Rose, M. J. Mehl, E. Perim, I. Takeuchi, S. Sanvito, M. Scheffler, Y. Lederer, O. Levy, C. Toher, and S. Curtarolo, *Journal of Chemical Information and Modeling* **58**, 2477 (2018).
- <sup>56</sup> W. Yuhasz, D. Schlager, Q. Xing, R. McCallum, and T. Lograsso, *J. Alloys Compd.* **492**, 681 (2010).
- <sup>57</sup> A. Çakır, M. Acet, U. Wiedwald, T. Krenke, and M. Farle, *Acta Materialia* **127**, 117 (2017).
- <sup>58</sup> T. Krenke, A. Çakır, F. Scheibel, M. Acet, and M. Farle, *J. Appl. Phys.* **120**, 243904 (2016).
- <sup>59</sup> V. Sokolovskiy, M. Gruner, P. Entel, M. Acet, A. Çakır, D. Baigutlin, and V. Buchelnikov, *Phys. Rev. Mater.* **3**, 084413 (2019).
- <sup>60</sup> M. Zayed, A. Elabbar, and O. Yassin, *J. Alloys Compd.* **737**, 790 (2018).
- <sup>61</sup> J. Zhou, B. Sa, Z. Sun, C. Si, and R. Ahuja, *RSC Adv.* **5**, 73814 (2015).
- <sup>62</sup> J. Zhang, X. Li, and J. Yang, *J. Mater. Chem. C* **3**, 2563 (2015).